



HAL
open science

Surface oxidation and phase transformation of the stainless steel by hybrid laser-waterjet impact

Laurent Weiss, M. Aillerie, Abdel Tazibt, Tidu Albert

► To cite this version:

Laurent Weiss, M. Aillerie, Abdel Tazibt, Tidu Albert. Surface oxidation and phase transformation of the stainless steel by hybrid laser-waterjet impact. *Materials Research Express*, 2014, 1 (3), pp.036501. 10.1088/2053-1591/1/3/036501 . hal-02421823

HAL Id: hal-02421823

<https://hal.science/hal-02421823v1>

Submitted on 20 Dec 2019

HAL is a multi-disciplinary open access archive for the deposit and dissemination of scientific research documents, whether they are published or not. The documents may come from teaching and research institutions in France or abroad, or from public or private research centers.

L'archive ouverte pluridisciplinaire **HAL**, est destinée au dépôt et à la diffusion de documents scientifiques de niveau recherche, publiés ou non, émanant des établissements d'enseignement et de recherche français ou étrangers, des laboratoires publics ou privés.

Surface oxidation and phase transformation of the stainless steel by hybrid laser-waterjet impact

To cite this article: L Weiss *et al* 2014 *Mater. Res. Express* 1 036501

Related content

- [Elimination of striation in laser cutting of mild steel](#)
M Sobih, P L Crouse and L Li
- [Case study of grate-chain degradation in a Grate-Kiln process](#)
Erik A A Nilsson, L Pettersson and M-L Antti
- [Fabrication of nano-sized grains by pulsed laser surface melting](#)

Recent citations

- [Surface and microstructure modifications of Ti-6Al-4V titanium alloy cutting by a water jet/high power laser converging coupling](#)

Surface oxidation and phase transformation of the stainless steel by hybrid laser-waterjet impact

L Weiss¹, M Aillerie², A Tazibt³ and A Tidu¹

¹Laboratoire d'Etude des Microstructures et Mécanique des Matériaux, UMR CNRS 7239, Ecole Nationale d'Ingénieurs de Metz, 1 route d'Ars Laquenexy, 57070 Metz, France

²Laboratoire Matériaux Optiques, Photonique et Systèmes, Université de Lorraine & Supélec, 2 rue Edouard Belin, Metz, France

³Centre de Recherche, d'Innovation et de Transfert Technologique en Jet Fluide, 2 Avenue de la Grande Terre 55000 Bar-le-Duc, France

E-mail: laurent.weiss@univ-lorraine.fr

Materials Research Express 1 (2014) 036501

Abstract

Hybrid jets (laser guided by water jet) are commonly used in the area of microelectronics for cutting thin wafer plates and for the design of special pieces. In this context, the hybrid jet works with a low power and low pressure. Efforts are made to apply and to improve this hybrid technology for cutting thicker metallic materials. In order to facilitate this development, we have studied the effects induced by a water jet–laser system coupled to the same point on a metallic material. The pressure of the water jet is about 1 MPa and the power of the laser source is about 400 W, which is much higher than the actual hybrid jet power. As a result, in the case of 301 L steel plates, we have noticed the formation of a magnetite layer around the cut in accordance with the high temperature reactions between water and iron, but, surprisingly, in this case, the reaction is practically instantaneous. A small percentage of hematite also appears, from a secondary reaction of reduction of magnetite. By using different techniques (Raman spectroscopy, optical microscopy, SEM, XRD...) we have observed, firstly, that the width of the oxidized zone is proportional to the cutting speed and on the other hand, that there exists a phase transformation in a small heat-affected zone, consistent with the hybrid jets literature.

Keywords: oxide formation, steel cutting, coupled laser-waterjet, phase transformation

1. Introduction

Description and understanding of the interactions between a fluid, light and matter at the interface between the three areas help to control surface changes related to these phenomena.

For fifteen years, several papers proposed to study those interactions using various processes. All these experiences can be classified into three main groups. The first one includes all experiments in which the sample is completely immersed with a laser that hits different materials targets. Sakka *et al* [1] have studied these interactions in the case of laser-ablation of graphite. The influence of a laser beam modulation on the etching rate of silicon/liquid interface has been described by Shafeev and Simakhin [2]. Alfile *et al* [3] have extensively studied the laser cutting process of steel. The second group includes configurations where the sample is immersed in a gaseous atmosphere with a laser hitting the material surface while a jet of water or steam is sent near to the area to cool it down or to interact chemically (Geiger *et al* [4]). The last group is formed by exotic interactions such as fluidic optical fiber on copper (Porter *et al* [5]) or silicon (Kraya *et al* [6]), waterfall on the material surface (Dupont *et al* [7]), fluid/air mix (Matsumoto *et al* [8]). All these experiments were reported by Kruusing [9–10]. Most of these works deal with materials such as polymers or ceramics. Thus, these studies focus on physical associated phenomena such as cracks, steam bubbles, surface activation and colloid formation. Few studies are about metal cutting and, among them, to our knowledge, none deals with the phase transformations and the emergence of surface oxides in a laser/water jet mixing. Fluidic optical fiber cutting, which has existed for a decade, allows cutting of thin materials (100 microns) because of low power and pressure used (100 W, 10 MPa). Engineers are currently working to increase the energy of the system to cut thick sheets while limiting the HAZ to interest the aeronautics industry.

That is why we propose to study here, for the first time, the structural effects of phase transformation during cutting of stainless steel with a ‘coupled water laser jet (WLJ) converging on the surface’ to be cut. This last approach, as will be described later in this paper, minimizes the interaction zone and allows rapid evacuation of the cutting residues.

The power provided by the laser is 400 W; the deposited energy greatly increases the reactivity of water molecules with the surface, resulting in the oxidation of the material under extreme conditions. Conditions created this way can form a layer of magnetite on the surface near the cutting area as shown by the results of XRD diffraction, Raman spectroscopy and electron microscopy.

As a first application, this process has been applied for austenitic stainless steel 301L. These are attractive materials for industrial applications requiring excellent corrosion resistance in combination with good mechanical properties. But it is well known that 301L stainless steel is subjected to phase transformation. Austenitic stainless steels have face-centred cubic (FCC) crystal structure. The stacking fault energy (SFE) of austenitic stainless steels is low and the austenite stability is strongly dependent on temperature and strain rate. During plastic deformation, depending on the stacking fault energy, we can observe the formation of strain-induced martensite phases, as shown by Curtze *et al* [11].

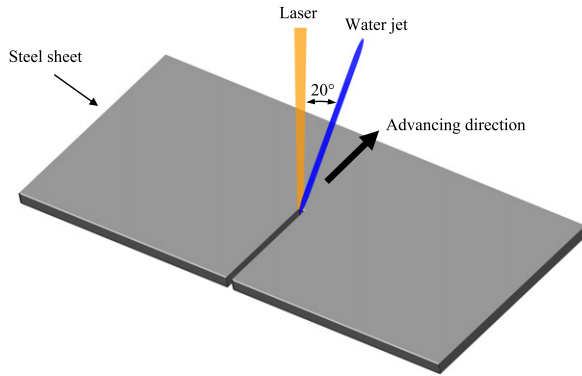


Figure 1. Schematic drawing of the cutting system.

Table 1. 301L steel chemical composition.

Element	Cr	Ni	Mn	Si	N	P	C	S
Content %	17.5	7	2	1	0.14	0.045	0.03	0.015

2. Material and experimental setup

The chemical composition of the 301L stainless steel used in this investigation is given in table 1.

The cold rolled sheet of 0.8 mm thickness is fixed on a moving cross-table following two axes X and Y . The water jet and the laser beam are fixed to a collimating/focusing system that can move perpendicularly to the top plane of the sample (along the Z axis). The light source is a continuous Yb:YAG disc laser with a 1030 nm wavelength. The lens has a 150 mm focal length that forms a 0.113 mm spot size. The water passes into a softener and a pump to be sent at 1 MPa through a 0.25 mm sapphire nozzle diameter. All components are standard and currently used in water jet cutting technology.

As shown in figure 1, both water jet and laser beam are focused at the same point on the surface of the sample to be cut. The laser beam arrives perpendicularly to the sheet and forms a 20° angle with the water jet. The feed rate vector is contained in the plane formed by water jet and laser beam. We have varied the cutting speed from 0.3 to 1.1 m min^{-1} rated in steps of 0.1 m min^{-1} . Following preliminary cutting tests, we have obtained that the optimal speed rate exists and is equal to 0.7 m min^{-1} . This optimal cutting speed leads to a minimum streak.

A tank located below the device allows the recovery of effluents (residues and water).

The presence of oxide and the expected phase transformations were studied by using two different techniques. The first one is the x-ray diffraction (XRD). The XRD equipment comprised a diffractometer D5000 equipped with a linear position sensitive detector and a chromium anode ($K_\alpha = 0.229 \text{ nm}$). The other characteristics are 0.034° step, 2 s acquisition time, 40 kV tension, 35 mA intensity, 0.8 mm collimator and a graphite monochromator.

To obtain more information about the oxides, the samples have been analyzed using Raman spectroscopy. The spectrometer is a LabRam Aramis at 532 nm focused by an X20 objective. This wavelength limits the appearance of fluorescence. The results are processed with the software Labspec.

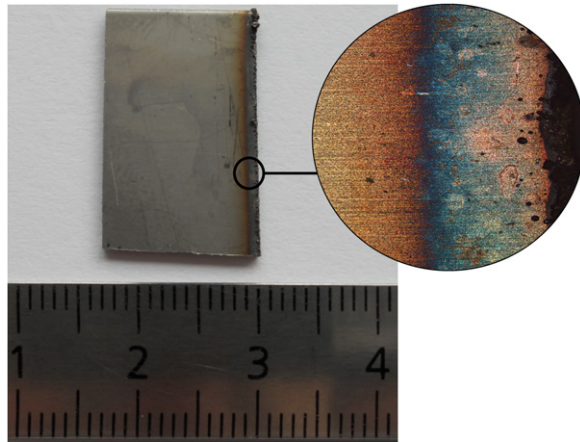


Figure 2. Macroscopic view of sample after cutting (0.4 m min^{-1} speed) and zoom on the oxidized zone (X5).

Finally, the samples were analyzed by scanning electron microscopy (SEM) using a Supra 40™ Carl Zeiss to study the heat affected zone, the expected phase transformation and the chemical composition. Grain orientations and phase crystallography were determined by electron back-scattered diffraction (EBSD), using the Channel 5 system (Oxford Instruments, HKL Technology) for data acquisition and analysis. The chemical compositions of the different phases present in the material were analyzed by energy-dispersive x-ray spectroscopy (EDX), using the Bruker Quantax system and the Spirit 1.8 software.

The samples were prepared using an electrochemical etching of 2 h consisting of 85 mL of ethanol, 5 mL of hydrochloric acid and 3 mL of nitric acid.

In addition, the cutting residues are carried by the jet and recovered after filtering in a tray. The obtained material is also analyzed after separating effluent and powders.

3. Experimental results and discussion

As observed during the cutting process and for the cutting to be effective, a first stage corresponds to the formation of an initial crater, accompanied by gas and material ejection. During the cutting process, the material adjacent to the zone of cut is rapidly heated and quenched, leading to the formation of a non-equilibrium temperature field propagating into the bulk. As a first observation, we can notice the presence of oxide on the surface of both wall sides of the kerf, as shown in figure 2.

The width of the oxidized zone ranges from 0.2 to 1.5 mm depending on the cutting speed. The 0.7 m min^{-1} speed has the best relationship between size of the oxidized zone and smear size. The higher the speed, the higher is the smear; the lower the speed, the higher is the oxidized area. This influence is shown in figure 3.

The linear decrease can be explained as follows: the laser brings enough energy to activate the oxidation reaction and to grow up the oxide layer. One can argue that lower is the speed, the higher is the thermal diffusion inside the material and the higher is the expansion of hot reactive zone between steel and water.

As confirmed by XRD analysis of the material before being cut, the 301L is an austenitic stainless steel. We can observe a residue of martensitic phase. XRD patterns, measured using

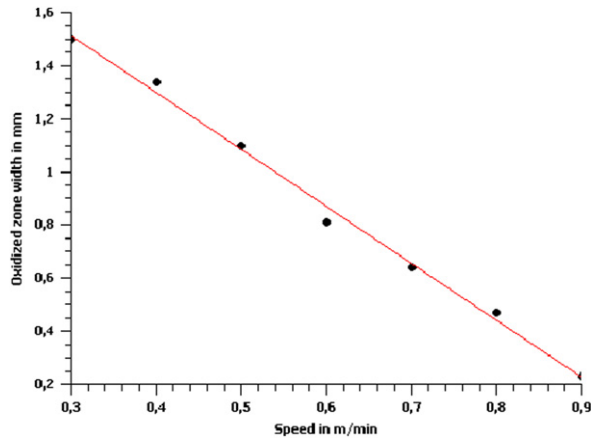


Figure 3. Evolution of the width of the oxidized zone as function of the cutting speed.

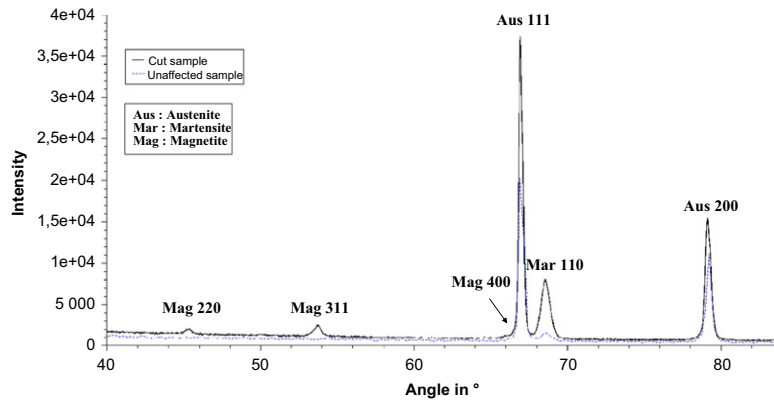


Figure 4. XRD pattern after cutting in the oxidised area.

integrated ϕ - Ψ measurement, show that the peaks of the austenite and martensite do not vary, meaning that the material is isotropic, i.e., without specific crystallographic texture.

The first step to determine the type of the created oxide is the XRD study of the material surface near the cutting edge. In figure 4, we note the appearance of magnetite (Fe_3O_4) peaks corresponding, for the first three peaks, to the (220), (311) and (400) diffracting planes as reported by Mahadevan *et al* [12] and Ren *et al* [13], respectively. One can notice a higher intensity of the (110) α' martensitic peak that means an increase of the martensitic phase amount.

The SEM microphotography (figure 5(a)) as well as the EBSD and phase maps (figures 5(b) and (c)) of the cutting area cross-section show the presence of martensite which results from the cutting process. These observations confirm that a martensitic transformation occurs near the cutting area leading to the formation of a metallurgical affected zone (MAZ). The water flow instantly cools the kerf area, which limits the HAZ width at most $100\ \mu\text{m}$ in the energy range used.

Thus, it is clear that during the cutting process, all the martensite is not reverted to austenite, as indicated by the higher amount of recorded martensite. As for the uncut material

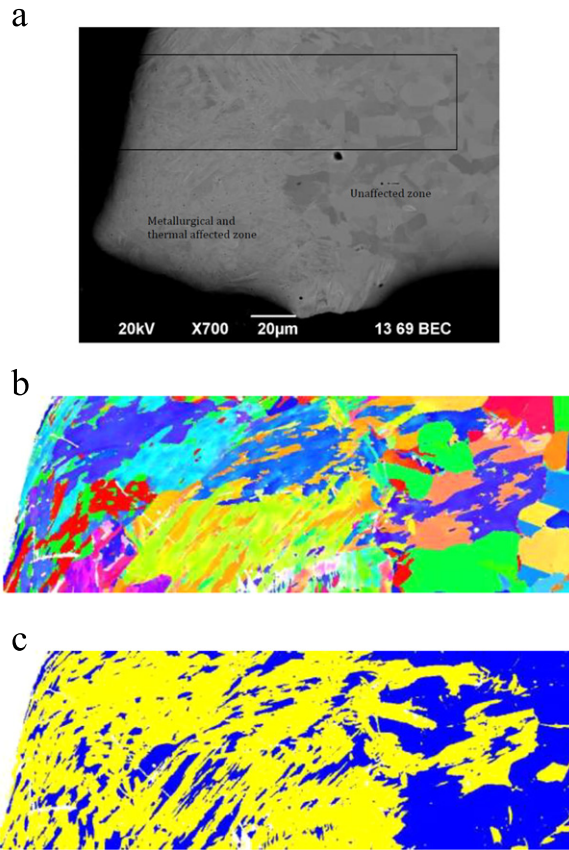


Figure 5. (a) SEM micrograph of the cross-section of the cutting area (b) EBSD map of the selected area (c) Phase indexation: martensitic in yellow and austenite in blue

(steel sample before being cut), using EBSD results, we do not observe any specific crystallographic texture for any phase.

Indeed, the water will react with the iron in the steel following the oxidation reaction (1):



Matthews [14] has described the formation of magnetite on steel in the presence of water. The laser heats the steel surface, and a part of this heat is transferred to the water which is transformed into vapor. The latter is very reactive with the steel and forms a layer of magnetite by oxidation of iron. But the reaction (1) is limited by the reaction (2) below. In fact, the magnetite can react again with water to produce hematite (Fe_2O_3) by reduction (2), as follows:



But as shown in figure 4, the hematite does not appear on the XRD diagram. So to validate this theory, we have used Raman spectroscopy. Figure 6 is a linear mapping of the surface of the sample from the cutting edge towards the center of the sample.

As we can see in figure 6, some Raman peaks appear next to the kerf and disappear slowly with the distance from the edge. The peaks field is 1.5 mm width in the sample cut at 0.3 m min^{-1} . This result matches the measurement obtained by optical microscopy given in figure 2. If we look more precisely at a slice of this mapping in the kerf zone, we can see that the peaks correspond to iron oxide (figure 7).

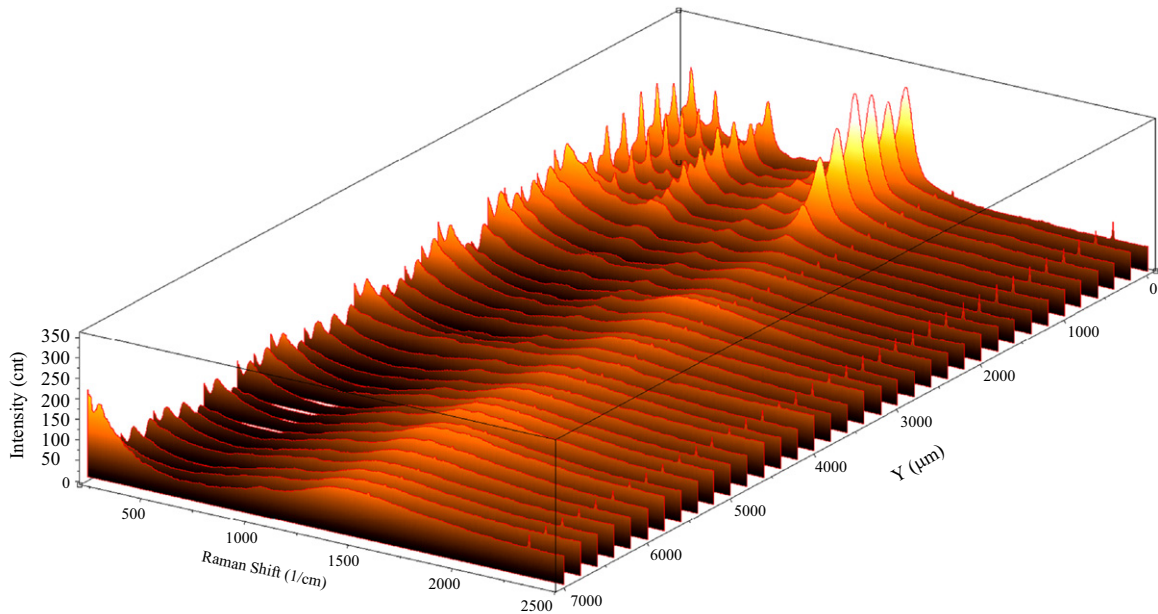


Figure 6. Linear mapping on the surface sample from the kerf towards the center of the sample (0.3 m min^{-1} speed).

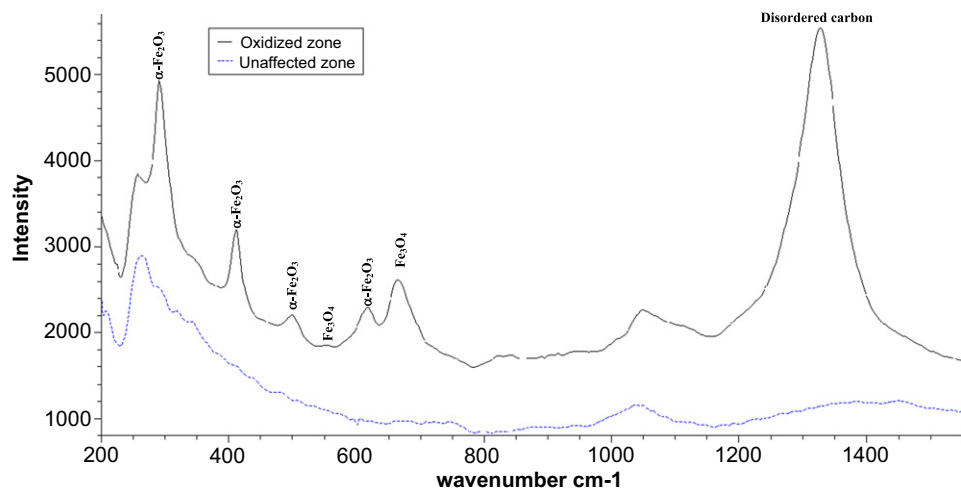


Figure 7. Comparison between Raman spectrum of oxidized and unaffected zone on the surface sample

Raman signature of magnetite was captured as well as that of hematite. The location of the different peaks corresponds to those found by de Faria *et al* [15] for natural magnetite. They correspond also with results obtained by Oblosky and Devine [16] for oxidized steel, by Dünwald and Otto [17] for oxidized steel in corrosive atmosphere and by Zeng *et al* [18] in the case of metal dusting. We have obtained for magnetite two characteristic peaks at 538 and 665 cm^{-1} and for hematite four main peaks at 291, 411, 499 and 615 cm^{-1} . Even if it is an aqueous environment, there is no formation of hydroxide, but in this area, in addition to these oxides, there is a formation of disordered carbon whose peak is located at 1326 cm^{-1} . Ferrari

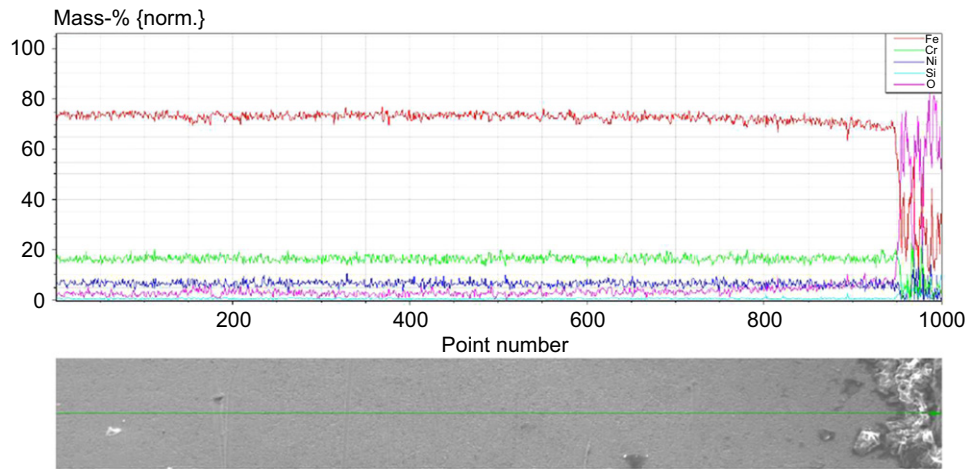


Figure 8. Linear chemical analysis on the cross-section across the MAZ (from the border to the core)

and Robertson [19–21] have calculated theoretically and demonstrated the presence of this disordered carbon peak around this point. The Raman scattering coefficient of carbon is much larger than for oxides. This fact explains the high intensity while the carbon content is very low.

An interesting fact is the absence of the signature of chromium oxide in the Raman spectra whose peaks have been detected by Maslar *et al* [22] and confirmed by Chen *et al* [23]. This result is consistent with the measured x-ray patterns despite 18% chromium in steel. EDS analysis was performed to check either the presence or the absence of chromium and the obtained results are given in the figure 8.

Only the oxygen content decreases when the distance increases from the cutting area; the chromium is still present in the oxidized zone and in the same proportions as in the core of the sample. The same observation is valid for the other metallic elements. Various studies on the corrosion of stainless steel under water atmosphere at high temperature have shown that chromium forms an oxide called chromite. Its formula is FeCr_2O_4 where nickel can replace either an iron or a chromium cation. As the chromite crystal parameters are really close to the magnetite, the XRD peaks are nearly the same for both. Concerning Raman results, Lister and co-workers [24] have shown that the chromium oxide is not located at the surface but in an internal layer. Raman spectroscopy measures only the first nanometers depth, which is why the chromite peaks are not seen in the spectra.

There are two other observations result from figure 6 as a function of the distance: the first one is the maximum peak width at half height; the second is the wavenumber shift of the peak (figures 9(a) and (b)).

Changes presented in figure 9 are the same for amorphous carbon, magnetite and hematite. When moving away from the cutting area, the peaks shift to higher frequencies, meaning that the vibration modes are limited. So the structure is less chaotic and more stressed. The increase of the peak width at half height means that the compounds are more evenly distributed in the matrix which forms a homogeneous mixture. The melted area and unaffected zone are visible in figure 5.

Due to thermal diffusion and oxidation reaction zone, the disordered structure extends along the upper and lower surface of the sample according to the Raman shift. These gathered

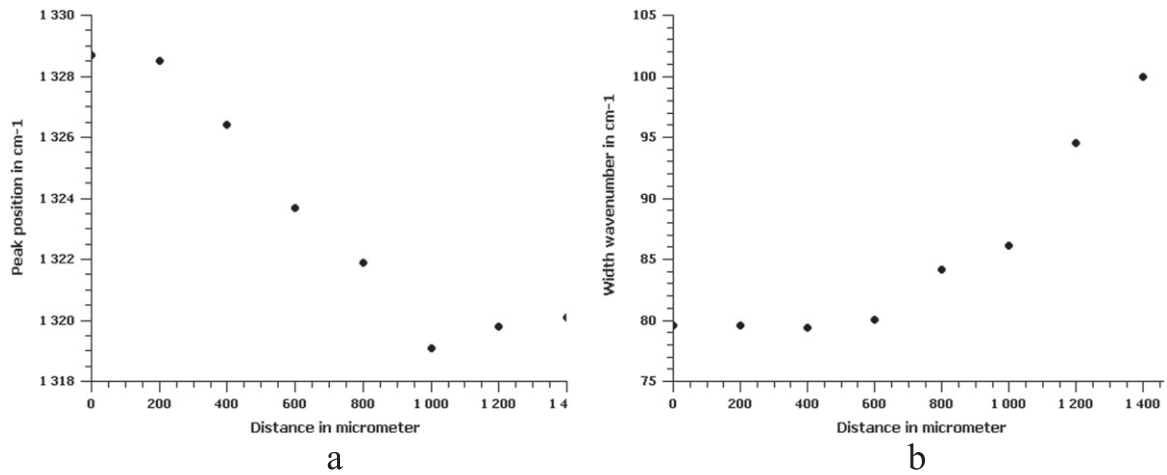


Figure 9. (a) Wavenumber shift of the amorphous carbon peak as function of the distance (b) Amorphous carbon peak width at half height as function of the distance

results constitute our conclusion about the phase formation and transformation on the cut sample. But what type of reaction takes place in the kerf where the material is removed? The response to this fundamental question can be given by a careful examination of the residue.

As shown in figure 10(a), the powder collected in the tray consists of microspheres meaning that the material was melted and was expelled by the water jet. These microspheres are composed mostly of magnetite and a smaller amount of hematite as confirmed by Raman spectra (figure 10(b)).

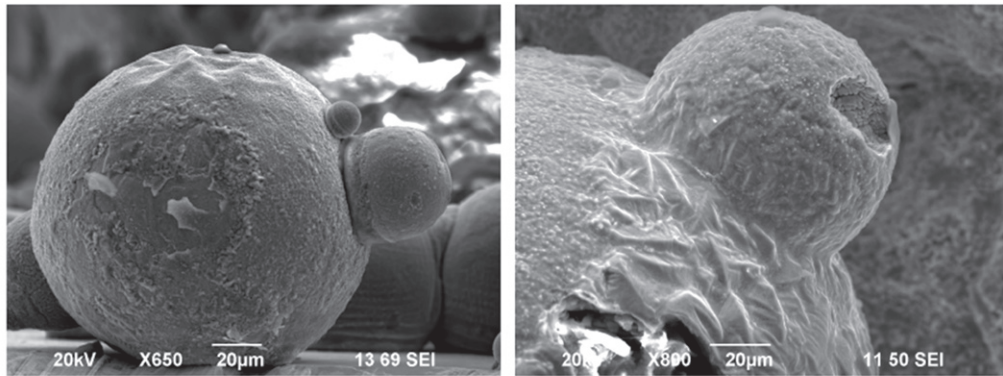
This composition can be explained by the fact that the limiting reduction reaction of magnetite can hardly take place because the powder is still in solution in the water and is no longer in the heat affected zone. The lack of hydrogen as a reagent results in only a trace of hematite. Many spheres can be seen on the sample, next to the kerf (figure 10(a)). They were expelled by the water jet but do not fall into the tray: they fall on the sample and merge with it.

One last thing to be noted is that the magnetite always takes a chaotic form: the crystals are mixed randomly (figure 11(a)). But when the feed rate is too high, the sample is not completely cut (dotted kerf). At this time, around the generated holes, we have observed euhedral magnetite (figure 11(b)). Those crystals are not ejected so they still to grow up slowly to a few hundred nanometres.

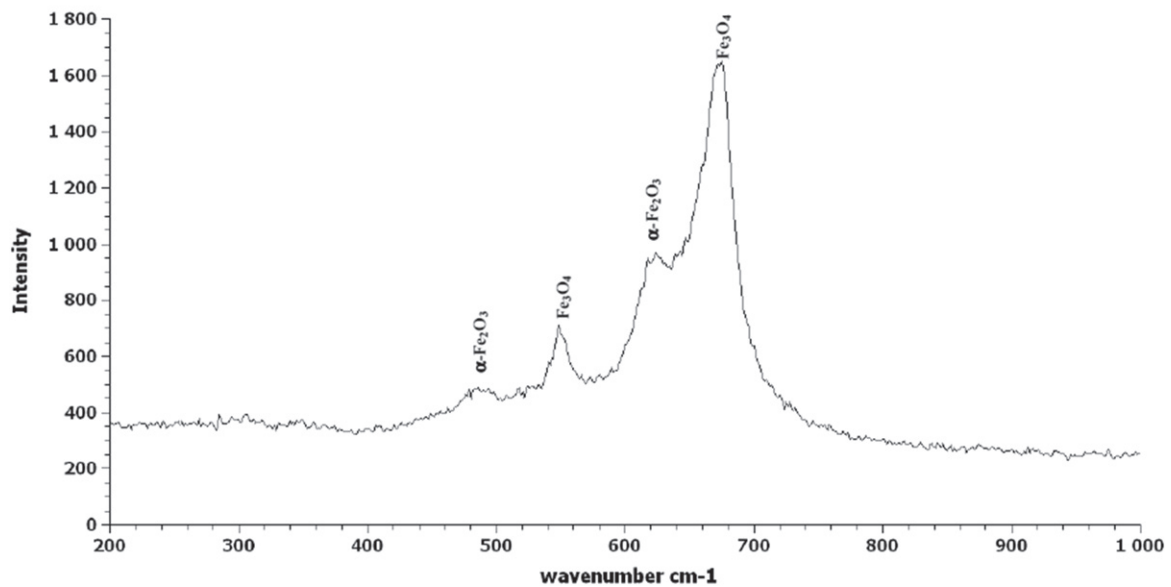
It is very difficult to compare the results of this study with a simple laser or water jet cutting. Indeed, in the case of the laser for example, a high pressure of neutral gas (argon, helium...) is necessary and does not cause chemical reaction on the surface. In our case, in view of the results, it appears that part of the energy supplied by the laser is not used to cut but is used to increase the kinetics of the formation of magnetite from iron and water. We have tested the laser alone and water alone but they have not cut; only the coupling allows the machining of the sheet.

4. Conclusion

We have designed and used a special water laser jet converging cutting system to simulate a high power hybrid jet. We can observe and explain several phenomena:



a



b

Figure 10. (a) Powder residues and magnetite powder fixed on the sample surface near the cutting edge. (b) Raman spectrum of powder.

- We have observed the formation of magnetite and hematite on the 301L sheet surface. These oxides are the reaction products of successive oxidation and reduction of iron in the presence of water. In our case, the oxides are instantly formed which means that a significant part of the laser energy is used to increase the reaction kinetics
- The linear evolution of the oxide width as function of the feed rate is due to the thermal diffusion
- Depending on the feed rate, magnetite is formed either chaotically or euhedrally. This advantage would allow our system to be used as a surface treatment to protect parts including localized protection against corrosion.
- It is possible that the formation of a large oxide layer at the kerf edge helps to cut by weakening the matrix.

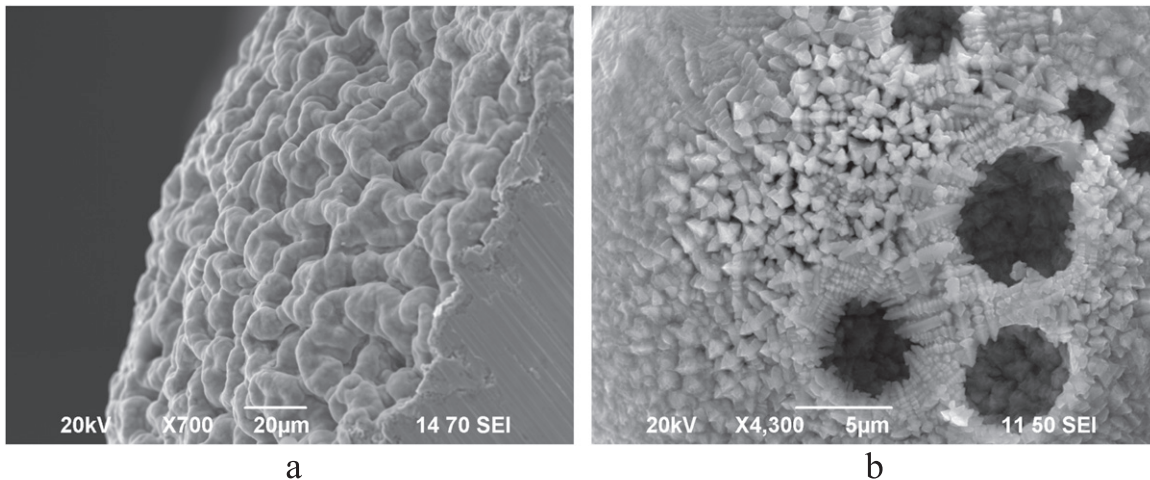


Figure 11. SEM pictures of chaotic and euhedral magnetite next to the kerf with: (a) 0.7 m min^{-1} speed (b) 11 m min^{-1} speed

- Raman spectroscopy has allowed showing the evolution of the stress into the microstructure of the oxidized zone and the homogeneity of the reaction products.

All of these results should be taken into account in the interest of increasing the laser power hybrid jets for cutting larger thicknesses. Further tests could be conducted to check the evolution of the reaction as a function of water jet pressure. We suggest extending this study to other materials and using other fluids than water to activate other reactions and therefore other surface treatments.

Acknowledgments

The authors wish to express their great gratitude to Dr Olivier Perroud (LEM3) and Ing. Daniel Knispel and Peggy Gressel from Institut de Soudure (Yutz, France) for their active participation in the experiments.

References

- [1] Sakka T, Iwanaga S, Ogata Y H, Matsunawa A and Takemoto T 2000 Laser ablation at solid–liquid interfaces: an approach from optical emission spectra *J. Chem. Phys.* **112** 8645–53
- [2] Shafeev G A and Simakhin A V 1992 Spatially confined laser-induced damage of Si under a liquid layer *Appl. Phys. A* **54** 311–6
- [3] Alfille J P, Pilot G and de Prunelle D 1996 New pulsed YAG laser performances in cutting thick metallic materials for nuclear applications *Proc. SPIE* **2789** 134–44
- [4] Geiger M, Becker W, Rebhan T, Hutfless J and Lutz N 1996 Increase of efficiency for the XeCl excimer laser ablation of ceramics *Appl. Surf. Sci.* **96** 301–15
- [5] Porter J A, Louhisalmi Y A, Karjalainen J A and Fügler S 2005 Cutting thin sheet metal with a water jet guided laser using various cutting distances, feed speeds and angles of incidence *Int. J. Adv. Manuf. Technol.* **33** 961–7
- [6] Kray D, Hopman S, Spiegel A, Richerzhagen B and Willeke G P 2007 Study on the edge isolation of industrial silicon solar cells with waterjet-guided laser *Sol. Energy Mater. Sol. Cells* **91** 1638–44

- [7] Dupont A, Caminat P and Bournot P 1995 Enhancement of material ablation using 248, 308, 532, 1064 nm laser pulse with a water film on the treated surface *J. Appl. Phys.* **78** 2022–8
- [8] Matsumoto O, Sugihar M and Miya K 1992 Underwater cutting of reactor core internals by CO laser using local-dry-zone creating nozzle *J. Nucl. Sci. Technol.* **29** 1074–9
- [9] Kruusing A 2004 Underwater and water-assisted laser processing: Part 1—general features, steam cleaning and shock processing *Opt. Lasers Eng.* **41** 307–27
- [10] Kruusing A 2004 Underwater and water-assisted laser processing: part 2—etching, cutting and rarely used methods *Opt. Lasers Eng.* **41** 329–52
- [11] Curtze S, Kuokkala V T, Oikari A, Talonen J and Hänninen H 2011 Thermodynamic modeling of the stacking fault energy of austenitic steels *Acta Mater.* **59** 1068–76
- [12] Mahadevan S, Gnanaprakash G, Philip J, Rao B P C and Jayakumar T 2007 X-ray diffraction-based characterization of magnetite nanoparticles in presence of goethite and correlation with magnetic properties *Physica E* **39** 20–5
- [13] Ren X, Sridharan K and Allen T R 2006 Corrosion of ferritic–martensitic steel HT9 in supercritical water *J. Nucl. Mater.* **358** 227–34
- [14] Matthews A 1976 Magnetite formation by the reduction of hematite with iron under hydrothermal conditions *Am. Mineral.* **61** 927–32
- [15] De Faria D L A, Venâncio Silva S and De Oliveira M T 1997 Raman microspectroscopy of some iron oxides and oxyhydroxides *J. Raman Spectrosc.* **28** 873–8
- [16] Oblosky L J and Devine T M 1995 A surface enhanced Raman spectroscopic study of the passive films formed in borate buffer on iron, nickel, chromium and stainless steel *Corrosion Sci.* **37** 17–41
- [17] Dünnwald J and Otto A 1989 An investigation of phase transitions in rust layers using Raman spectroscopy *Corrosion Sci.* **29** 1167–76
- [18] Zeng Z, Natesan K and Maroni V A 2002 Investigation of metal-dusting mechanism in Fe-base alloys using raman spectroscopy, x-ray diffraction and electron microscopy *Oxid. Met.* **58** 147–70
- [19] Ferrari ac and Robertson J 2000 Interpretation of Raman spectra of disordered and amorphous carbon *Phys. Rev. B* **61** 14095–107
- [20] Ferrari ac and Robertson J 2001 Resonant Raman spectroscopy of disordered, amorphous and diamondlike carbon *Phys. Rev. B* **64** 075414
- [21] Ferrari ac and Robertson J 2004 Raman spectroscopy of amorphous, nanostructured, diamond-like carbon and nanodiamond *Phil. Trans. R. Soc. A* **362** 2477–512
- [22] Maslar J E, Hurst W S, Bowers W J, Hendricks J H, Aquino M I and Levin I 2001 *In-situ* Raman spectroscopic investigation of chromium surfaces under hydrothermal conditions *Appl. Surf. Sci.* **180** 102–18
- [23] Chen M, Shu J and Mao H-K 2008 Xieite a new mineral of high-pressure FeCr₂O₄ polymorph *Chin. Sci. Bull.* **58** 3341–5
- [24] Lister D H, Davidson R D and McAlpine E 1987 The mechanism and kinetics of corrosion product release from stainless steel in lithiated high temperature water *Corrosion Sci.* **27** 113–40